Title

The 4-N-acyl and 4-N-alkyl gemcitabine analogues with silicon-fluoride-acceptor: Application to 18F-Radiolabeling

Authors

Gonzalez, Cesar
Sanchez, Andersson
Collins, Jeffrey
et al.

Publication Date

2018-03-01

DOI

10.1016/j.ejmech.2018.02.017

Peer reviewed

HHS Public Access

Author manuscript

Eur J Med Chem. Author manuscript; available in PMC 2019 March 25.

Published in final edited form as:

Eur J Med Chem. 2018 March 25; 148: 314–324. doi:10.1016/j.ejmech.2018.02.017.

The 4-*N*-Acyl and 4-*N*-Alkyl Gemcitabine Analogues with Silicon-Fluoride-Acceptor: Application to ^{18}F-Radiolabeling

Cesar Gonzalez[†], **Andersson Sanchez**[†], **Jeffrey Collins**[‡], **Ksenia Lisova**[‡], **Jason T. Lee**[‡], **R. Michael van Dam**[‡], **M. Alejandro Barbieri**[§], **Cheppail Ramachandran**[‖], and **Stanislaw F. Wnuk**[*,†]

[†]Department of Chemistry and Biochemistry, Florida International University, Miami, Florida 33199, United States

[‡]Crump Institute for Molecular Imaging, Department of Molecular and Medical Pharmacology, Los Angeles, California, United States

[§]Department of Biological Sciences, Florida International University, Miami, Florida 33199, United States

[‖]Nicklaus Children's Hospital, Miami, Florida, United States

Abstract

The coupling of gemcitabine with functionalized carboxylic acids using peptide coupling conditions afforded 4-*N*-alkanoyl analogues with a terminal alkyne or azido moiety. Reaction of 4-*N*-tosylgemcitabine with azidoalkyl amine provided 4-*N*-alkyl gemcitabine with a terminal azido group. Click reaction with silane building blocks afforded 4-*N*-alkanoyl or 4-*N*-alkyl gemcitabine analogues suitable for fluorination. RP-HPLC analysis indicated better chemical stability of 4-*N*-alkyl gemcitabine analogues versus 4-*N*-alkanoyl analogues in acidic aqueous conditions. The 4-*N*-alkanoyl gemcitabine analogues showed potent cytostatic activity against L1210 cell line, but cytotoxicity of the 4-*N*-alkylgemcitabine analogues was low. However, 4-*N*-alkanoyl and 4-*N*-alkyl analogues had comparable antiproliferative activities in the HEK293 cells. The 4-*N*-alkyl analogue with a terminal azide group was shown to be localized inside HEK293 cells by fluorescence microscopy after labelling with Fluor 488-alkyne. The [^{18}F]4-*N*-alkyl or alkanoyl silane gemcitabine analogues were successfully synthesized using microscale and conventional silane-labeling radiochemical protocols. Preliminary positron-emission tomography (PET) imaging in mice showed the biodistribution of [^{18}F]4-*N*-alkyl to have initial concentration in the liver, kidneys and GI tract followed by increasing signal in the bone.

[*]**Corresponding Author Information**. Telephone 30348-6195; wnuk@fiu.edu.

Supplementary Material. Detailed synthesis and characterization data for 11-azidoundecanoic acid (**S4**), 7-azido-1-aminoheptane (**S7**), 4-(azidomethyl)phenyldiiso-propylsilane (**S9**) and diisopropyl(4-((prop-2-yn-1-yloxy)methyl)phenyl)silane (**S10**) as well as experimental radiochemical and biological procedures, representative HPLC chromatograms, and stability and metabolite analysis protocols can be found at https://.

Graphical abstract

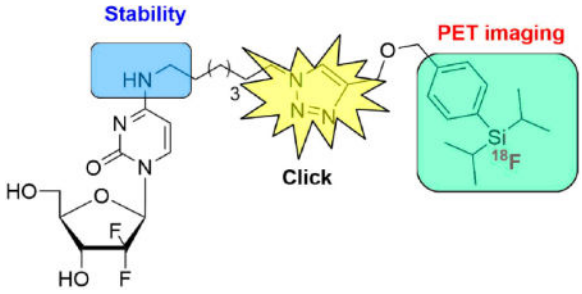

1. Introduction

Gemcitabine (2′,2′-difluoro-2′-deoxycytidine, dFdC), is a chemotherapeutic nucleoside analogue used as first line therapy in pancreatic and lung cancers.[1] Gemcitabine, like many other nucleosides, enters cells via the human equilibrative nucleoside transport protein 1 (hENT1) and is subsequently activated via phosphorylation by deoxycytidine kinase (dCK) and other kinases to its triphosphate form.[2, 3] The triphosphate is a substrate for DNA synthesis inhibiting DNA polymerase by chain termination during replication and repair processes, triggering apoptosis.[4]

Gemcitabine, even if beneficial for the treatment of a variety of tumors, can have its efficacy diminished by increased toxicity to normal cells and rapid intracellular deamination into inactive 2′,2′-difluorouridine (dFdU) by cytidine deaminase (CDA).[5–7] In order to tackle these issues, various prodrug strategies have been developed through hydrolysable lipophilic acyl modifications on the exocyclic 4-*N*-amine or 5′-hydroxyl group of the nucleoside,[8–14] and such approaches were recently reviewed.[15] These modifications facilitate the uptake by cells slowing also the release of gemcitabine through hydrolysis, which increases its bioavailability while also providing resistance to enzymatic deamination by CDA. Gemcitabine analogues have been also designed and synthesized as theranostic delivery systems with cellular specificity and imaging capabilities.[16–20] Increased bioavailability of gemcitabine 4-*N*-alkyl analogues have been scarcely explored and thus their synthesis and mode of activity need further investigation. Recently, Pulido et al. showed that 4-*N*-alkyl analogues had modest cytostatic activity with neither measurable deamination nor conversion to gemcitabine observed.[21, 22] This increased stability of the 4-*N*-alkyl analogues within the cell, compared to 4-*N*-alkanoyl counterparts, provides an opportunity for their development as novel derivatives of gemcitabine and to study their distribution via PET.

Although ^{18}F-radiolabeling has progressed tremendously in recent years, the incorporation of the fluorine-18 label into biomolecules normally involves a large number of steps and burdensome labeling procedures.[23–28] This is definitely the case in the synthesis of ^{18}F-labelled nucleoside analogues, which usually involves multiple protection and deprotection steps, and therefore can lead to an overall increased reaction time and decreased radiochemical yield. Since practical syntheses of gemcitabine analogues are based on incorporation of a *geminal* difluoro unit in their early synthetic stages,[29, 30] preparation of

2′-[^{18}F]dFdC is not feasible due to short half-life of the ^{18}F isotope.[31] Recently, the gemcitabine analogue 1-(2-deoxy-2-[^{18}F]fluoro-β-D-arabinofuranosyl)cytosine ([^{18}F]FAC) was developed enabling noninvasive prediction of tumor responses to gemcitabine and is utilized as a probe for PET imaging of dCK activity.[32–34] Although FAC generally follows the known *ex vivo* biodistribution of gemcitabine, it is missing a *geminal* difluoromethylene unit at C2′ which is reported to be critical for anticancer properties of dFdC and its inhibitory activity of ribonucleotide reductases.[35] Therefore, we have undertaken efforts to investigate dFdC derivatives with the geminal difluoro unit already incorporated and having a silane moiety that would allow convenient ^{18}F labelling.

The use of compounds bearing Si-F bond in radiochemistry has been explored since 1958,[36] with *in vivo* studies reported as early as the 1970s.[37] The Si-F bond was considered as an alternative to C-F bonds due to its increased bond strength (565 kJ/mol for Si–F versus 485 kJ/mol for C–F).[38] However, early on, it was discovered that even with this increased stability, the Si-F bond is highly susceptible to hydrolysis in physiological conditions.[38] This tendency can be prevented by the use of bulky substituents on Si-atom since they have been shown to shield the Si-F bond from hydrolysis while also increasing lipophilicity. This makes these silicon-fluoride acceptors potential ^{18}F-labeled tracers for PET imaging.[39–43] Herein, we report synthesis of clickable 4-*N*-alkanoyl and 4-*N*-alkyl gemcitabine analogues with silicon-fluoride acceptors, high-yield ^{18}F-radiolabeling via a conventional and micro-droplet approach, *in vitro* anti-cancer and cell localization evaluation, and preliminary *in vivo* biodistribution studies with PET imaging.

2. Results and Discussion

2.1. Chemistry

2.1.1 Synthesis of silane precursors—The strategy for the synthesis of gemcitabine analogues bearing silicon fluoride acceptors attached to an exo-amino group of cytosine ring involve: (a) synthesis of gemcitabine analogues having terminal azido or alkyne group at an alkyl chain attached to 4-amino group, and (b) copper(I) catalyzed click reaction with the corresponding silane reagent having terminal alkyne or azido group. Thus, condensation of gemcitabine **1** with 11-azidoundecanoic acid **S4** under peptide coupling conditions [(*N*-dimethylaminopropyl)-*N*′-ethyl-carbodiimide (EDC)/1-hydroxybenzotriazole (HOBt)/*N, N*-Diisopropylethylamine (DIPEA)] in DMF at 65°C afforded 4-*N*-(11-azidoundecanoyl)gemcitabine **2** (70%; Scheme 1). The 11-azidoundecanoic acid **S4** was prepared by esterification of the commercially available 11-bromoundecanoic acid and subsequent azidation (NaN_3/DMF) followed by saponification with the overall 81% yield (Scheme S1, see Supporting Information Section). Condensation of **1** with 5-hexynoic acid under similar conditions gave 4-*N*-(hexynoyl)gemcitabine **3** in lower yield contaminated with mono and/or di sugar 5-hexynoate esters. However, transient protection[44] of **1** with trimethylsilyl group followed by condensation with 5-hexynoic acid in the presence of EDC provided **3** (63%).

Copper-catalyzed click reaction of alkyne **3** with azido building block **S9** [4-(azidomethyl)phenyldiisopropylsilane] in the presence of sodium ascorbate and copper(I) sulfate gave silicon-fluoride acceptor **4** (92%). Alternatively azide **2** coupled with alkyne

building block **S10** [diisopropyl(4-((prop-2-yn-1-yloxy)methyl)phenyl)silane] gave **5** (87%). The two bifunctional silicon building blocks **S9** and **S10** were prepared from 4-(diisopropylsilyl)benzylalcohol **S8** as depicted in Scheme S3 (see SI section).

The synthesis of the 4-*N*-alkyl gemcitabine analogues with silicon-fluoride acceptor are based on displacement of a 4-*N*-tosylamine group from **7** with freshly prepared 7-azidohepylamine **S7**. Thus, transient protection of gemcitabine **1** with trimethylsilyl group and subsequent treatment with TsCl followed by deprotection with methanolic ammonia afforded 4-*N*-tosylgemcitabine[21] **7** (90%, Scheme 2). Treatment of **7** with 7-azidohepylamine **S7** effected displacement of the *p*-toluenesulfonamido group from the C4 position of the cytosine ring to give 4-*N*-(7-azidoheptanyl) gemcitabine **8** (82%). The 7-azidoheptylamine **S7** was prepared from 1,7-dibromoheptane by treatment with 2 eq. of NaN_3, followed by selective Staudinger reduction of one of the azido group in intermediary 1,7-diazidoheptane **S6** with triphenylphosphine in 83% overall yield (Scheme S2, see SI section). Click reaction of azido **8** with alkyne building block **S10** gave silane **9** (90%).

2.1.2. Fluorination and stability of Si-F products—Treatment of 4-*N*-acyl silanes **4** or **5** with KF in the presence of 18-crown-6 in MeCN at 80 ºC for 20 min followed by quick cooling, filtration, and silica column chromatography (5 → 10% MeOH/$CHCl_3$) gave the respective fluorinated products **11** (65%) or **6** (63%, Scheme 1). Analogous fluorination of 4-*N*-alkyl silanes **9** afforded (fluoro)diisopropylsilane **10** (62%, Scheme 2). Besides desired silyl fluorides **6**, **10** and **11** the corresponding silanols resulting from the hydrolysis from Si-OH were also isolated during purification on column (~20–25%). The structure of the silanols were confirmed by the absence of hydrogen from of Si-H bond (e.g., in **5** at 3.92 ppm) and lack of fluorine signal (e.g., in **6** at −188.86 ppm) in ^{1}H or ^{19}F NMR and additionally defined by HRMS.

Stability of 4-*N*-alkanoyl **5** and 4-*N*-alkyl **9** substrates as well as their fluorinated products **6** and **10** were examined employing RP-HPLC with isocratic mobile phase of CH_3CN/water containing 0.1% of TFA which is compatible with the purification protocols for the [^{18}F]-labeled products (*vide infra*). The 4-*N*-alkanoyl **5** were found to be prone to hydrolysis of the amide bond. For example, gemcitabine (10–15%, 30 min) was detected after **5** was dissolved in 35% CH_3CN/0.1% TFA (Figure 1). The RP-HPLC of the fluoro product **6** showed both hydrolysis of the acyl chain to gemcitabine (15%, 30 min) and Si-F bond to the corresponding silanol (20%, 30 min; Figure S1, see SI section). HPLC after 2 h showed larger amounts of silanol (30%) and gemcitabine (20%; Figure S2).

On the other hand, the 4-*N*-alkyl substrate **9** was found to be stable with only very minor formation of byproduct peak(s) (e.g., gemcitabine) observed after long exposure (8 h) to 35% CH_3CN/0.1% TFA (Figure S3, see SI). The fluorinated product **10** in the 25% CH_3CN/0.1% TFA in water hydrolyzes to silanol (25%, 1 h, 55%, 3 h; Figure S4). However, hydrolysis of **10** in TFA-free system (25% CH_3CN/water) occurred to a lesser extent (20%, 1 h, 30%, 3 h; Figure S5). These studies show that 4-*N*-alkyl analogues are more stable under acidic conditions than 4-*N*-acyl counterparts, indicating their advantage in developing them as PET imaging agents for gemcitabine prodrugs.

2.1.3. Radiosynthesis of [^{18}F]Fluoro-silane probes—The *conventional* one-pot syntheses of 4-*N*-alkanoyl [^{18}F]**6** and 4-*N*-alkyl [^{18}F]**10** were performed on the ELIXYS FLEX/CHEM radiosynthesizer employing silane-labeling protocols.[42] Thus, by adding silane precursor **9** in DMSO with 1% v/v AcOH to the previously dried [^{18}F]KF/K_{222} complex and reacting at 100°C for 25 min, followed by HPLC purification, 4-*N*-alkyl [^{18}F]**10** was produced with 6.6 ± 3.2 % (n = 5) decay-corrected isolated radiochemical yield and >99% radiochemical purity (Scheme 3, Table 1, Figure 2; see SI for more detailed protocols, Figure S6). Analogously, the ^{18}F-fluorination of precursor **5** gave 4-*N*-alkanoyl [^{18}F]**6** in ~0.5% (n = 1) decay-corrected crude radiochemical yield. Optimization of the protocol for the synthesis of [^{18}F]**6** was not performed.

The [^{18}F] labeled **6** and **10** were synthesized more efficiently using microscale approach on simple microfluidic chips (Figure S7 in SI).[45, 46] By adding silane precursor **5** or **9** in DMSO with 1% v/v AcOH to the previously dried [^{18}F]KF/K_{222} residue on one chip, covering with a second chip, and heating at 100 °C for 20 min, a decay-corrected crude radiochemical yield (i.e. without purification) for 4-*N*-alkanoyl [^{18}F]**6** was 10% (n = 1) and for 4-*N*-alkyl [^{18}F]**10** was 24.4 ± 4.1 (n = 5) (Figure S8, see SI for more detailed protocol). Additionally, 4-*N*-alkyl [^{18}F]**10** is radiochemically stable at ambient temperature for over 4 hours after formulation in saline with 10% v/v EtOH, with no significant radiolysis or other degradation observed (Figure S9, see SI).

2.2. Biological evaluation and imaging

2.2.1. Cytostatic activity—The antiproliferation capabilities of the 4-*N*-alkanoyl (**2**, **3**, **5** and **6**) and 4-*N*-alkyl (**8** and **9**) gemcitabine analogues were assessed (72 h) in L1210 mouse lymphocytic leukemia cells (Table 2). The 4-*N*-alkanoyl analogues **2** and **5** demonstrated potent antiproliferative activities with IC_{50} = 8.0 μM and IC_{50} = 7.5 μM, respectively. The reported IC_{50} value of gemcitabine for an identical incubation time (72 h) is 23.7 μM.[47] Derivatives **2** and **5** have also comparatively low IC_{75} values indicating superior antiproliferative effects. However, 4-*N*-alkylgemcitabine derivatives **8** and **9** showed less antiproliferative activities having IC values of >200 μM**.**

Additionally, we tested proliferation of human embryonic kidney HEK293 cells (48h) with 4-*N*-alkanoyl **2** and **5** and 4-*N*-alkyl analogues **8** and **9**. These analogues were found to have different levels of inhibition in a dose dependent manner and blocked cell proliferation (Table 3). These results show *comparable* antiproliferative activities for 4-*N*-alkanoyl and 4-*N*-alkyl analogues. This might be due to the fact that HEK293 cells have higher CDA activity than that reported for many other cells and organs;[48, 49] and that CDA expression/activity is known to affect anticancer therapy.[50],[51] Also, the low cytotoxicity of or high resistance to cytidine analogues such as gemcitabine have been associated with high levels of CDA expression in cancer cells.[52, 53] Conversely, the fact that 4-*N*-alkyl cytidine analogues (including 4-*N*-alkyl analogues of gemcitabine) are not substrates of CDA[22, 54] can contribute to their cytotoxicity in HEK293 cells since their metabolism to inactive uracil metabolites is either very slow or prohibited.

Even though 4-*N*-alkyl analogues **8** and **9** showed lower cytotoxic activities in the cells tested, we decided to study cellular uptake of **8** with HEK293 cells since the lipophilic[55] 4-*N*-alkyl derivatives of gemcitabine show a stability toward fluorination protocols compatible with ^{18}F fluorination. We were interested to investigate whether nucleoside **8** would be internalized and/or localized in the nucleus of cells and incorporated into DNA, or they are trapped in an extranuclear compartment.

To determine whether 4-*N*-alkyl analogue **8** was localized inside cells, we carried out *in vitro* fluorescence studies with HEK293 cells. The cells were incubated with 100 μM of **8** for 24 h, fixed and labelled with Fluor 488-alkyne in presence of copper (I). Fluor 488-labeled cells (Figure 3, B; seen in green) was evidence that 4-*N*-alkyl **8** was internalized by the cells.[56] Also, strong nuclear staining was evident by its co-localization with DAPI (Figure 3, A; seen in blue), as well as on the DNA during cell division. As expected, when cells were incubated without **8** no fluorescent green signal was observed (data not shown).

2.2.2. In Vivo Imaging of [^{18}F]4-N-alkyl gemcitabine radioligand 10—To determine the distribution and uptake of [^{18}F]**10**, preliminary *in vivo*, static and dynamic PET imaging studies were performed in wild-type mice. For static PET imaging, a WT C57BL/6 mouse was injected with [^{18}F]**10** via tail vein and imaged for 10 min after 1 h uptake. For dynamic PET imaging, a 1 h PET acquisition was started concurrently at the beginning of a 10 sec infusion via a tail vein catheter of [^{18}F]**10** and histogrammed into a series of images (Figures S10 and S11 in SI). Both static and dynamic PET imaging show the tracer first in the liver, kidneys, and GI tract (also the gallbladder in the static scan), but significant bone signal is evident after 15–20 min post-injection (Figure 4 and 5, see SI for more detailed protocol). One cause of bone signal is *in vivo* defluorination of the PET tracer, releasing [^{18}F]fluoride, which is strongly incorporated into hydroxyapatite crystals of bone. More detailed analysis of tracer metabolites *in vivo* is needed to determine whether defluorination is occurring or whether bone signal is actually uptake in bone marrow.

It appears that [^{18}F]4-*N*-alkyl gemcitabine radioligand **10** undergoes renal (high kidney, bladder) and possibly hepatobiliary (high gut and liver) clearances, with possible defluorination. It is noteworthy that biodistribution of the 4-N-alkyl radioligand does not reflect biodistribution of [^{14}C]gemcitabine.[5]

3. Conclusion

We have demonstrated that copper(I) catalyzed click reaction of the 4-*N*-alkanoyl or alkyl gemcitabine analogues having terminal azide or alkyne group on the alkyl chain with the silane reagents having terminal alkyne or azido group provided 4-*N*-alkanoyl and alkyl gemcitabine analogues with silicon-fluoride acceptors. RP-HPLC analysis showed that the 4-*N*-alkyl analogues were more stable in aqueous acidic conditions, indicating their advantage in developing them as PET imaging tracers. The silane 4-*N*-alkyl precursor **9** was successfully fluorinated to [^{18}F]**10** using conventional and microscale radiosynthetic methods in high radiochemical purity and stability of up to 4 h. Preliminary static and dynamic PET studies in wild-type mice have shown the initial biodistribution of [^{18}F]4-*N*-alkyl tracer **10** in the liver, kidneys and GI tract followed by increasing signal in the bone.

The 4-*N*-alkanoylgemcitabine analogues showed more potent antiproliferative activity in L1210 cells compared to the 4-*N*-alkylgemcitabine derivatives. However, 4-*N*-alkanoyl and 4-*N*-alkyl analogues had comparable antiproliferative activities in the HEK293 cells, which have high levels of CDA expression. The 4-*N*-alkyl gemcitabine derivatives were shown to be localized inside HEK293 cells by fluorescence microscopy after click labelling with Fluor 488-alkyne. The chemical and enzymatic stabilities of 4-*N*-alkylcytidine analogues and their compatibility with ^{18}F-labeling provide a potential avenue for developing new PET imaging tracers for gemcitabine derivatives. Future work would involve optimizing the structure to improve the *in vivo* stability and the biodistribution of these analogs.

4. Experimental Section

The ^{1}H (400 MHz), ^{13}C (100 MHz), or ^{19}F (376 MHz) NMR spectra were recorded at ambient temperature in solutions of $CDCl_3$ or MeOH-d_4 as noted. The reactions were followed by TLC with Merck Kieselgel 60-F_{254} sheets and products were detected with a 254 nm light or with Hanessian's stain. Column chromatography was performed using Merck Kieselgel 60 (230–400 mesh). Reagent grade chemicals were used and solvents were dried by reflux distillation over CaH_2 under nitrogen gas, unless otherwise specified, and reactions carried out under N_2 atmosphere. The carboxylic acid and amine derivatives used for the coupling with gemcitabine were commercially available or synthesized [11-azidoundecanoic acid (**S4**) and 7-Azido-1-aminoheptane (**S7**)] as described in Supporting Information. The purity of some of the synthesized compounds was determined by HPLC on Phenomenex Gemini RP-C18 with isocratic at various mobile phases (CH_3CN/H_2O) and flow rates.

4-*N*-(11-Azidoundecanoyl)-2′-deoxy-2′,2′-difluorocytidine (2)

N,*N*-Diisopropylethylamine (35 μL, 26 mg, 0.2 mmol), 1-hydroxybenzotriazole (27 mg, 0.2 mmol), **S4** (46 mg, 0.2 mmol), and 1-ethyl-3-(3-dimethylaminopropyl)carbodiimide (45 μL, 31 mg, 0.2 mmol) were sequentially added to a stirred solution of gemcitabine hydrochloride (**1**; 50 mg, 0.17 mmol) in DMF (4 mL) at ambient temperature under N_2 atmosphere The reaction mixture was then gradually heated to 65 °C (oil-bath) and was kept stirring overnight. The crude mixture was evaporated and the residue column chromatographed (0 → 10% MeOH/$CHCl_3$) to give **2** (56 mg, 70%): UV (CH_3OH) λ max 299 nm (ε 6500), λ min 250 nm (ε 12 900); ^{1}H NMR (CD_3OD) δ 1.24–1.47 (m, 12H, 6 × CH_2), 1.51–1.75 (m, 4H, 2 × CH_2), 2.45 (t, *J* = 7.4 Hz, 2H, CH_2), 3.27 (t, *J* = 6.9 Hz, 2H, CH_2), 3.81 (dd, *J* = 2.8, 12.4 Hz, 1H, H5′), 3.89–4.05 (m, 2H, H5″, H4′), 4.30 (td, *J* = 8.5, 12.2 Hz, 1H, H3′), 6.17–6.35 (m, 1H, H1′), 7.50 (d, *J* = 7.6 Hz, 1H, H5), 8.34 (d, *J* = 7.6 Hz, 1H, H6); ^{13}C NMR δ 25.92, 27.80, 29.90, 30.11, 30.20, 30.33, 30.41, 30.50, 38.17, 52.47, 60.30 (C5′), 70.27 (dd, *J* = 22.2, 23.6 Hz, C3′), 82.92 (d, *J* = 8.6 Hz, C4′), 86.42 (dd, *J* = 26.6, 37.6 Hz, C1), 98.25 (C5), 120.87 (t, *J* = 259.9 Hz, C2′), 145.96 (C6), 157.68 (C2), 164.83 (C4), 176.00 (CO); ^{19}F NMR δ −120.05 (d of m, *J* = 239.7 Hz, 1F), −119.10 (d of m, *J* = 240.1 Hz, 1F). HRMS (ESI+) *m/z* calcd for $C_{20}H_{30}F_2N_6NaO_5$ $[M+Na]^+$ 495.2146; found 495.2141.

4-*N*-(5-Hexynoyl)-2′-deoxy-2′,2′-difluorocytidine (3)

Trimethylsilyl chloride (250 μL, 2 mmol) was added to a solution of **1** (200 mg, 0.7 mmol) in MeCN (2 mL) and pyridine (3 mL) at 0 °C. The mixture was stirred for 4 h from 0 °C to room temperature. A solution of commercially available 5-hexynoic acid (230 μL, 2.1 mmol) in MeCN (2 mL), previously activated by EDC (50 μL, 1 mmol), was added to the reaction mixture, which was heated at 60°C for 18 h. After the solution was cooled down to room temperature, ethanol (5 mL) was added and the mixture was heated at 45 °C for 4 h. After evaporation under vacuum, the resulting residue was column chromatographed (80 → 100% EtOAc/hexane) to give **3**[44] (157.6 mg, 63%): ^{1}H NMR (CD_3OD) δ 1.84–1.86 (m, 2H, CH_2), 2.26–2.28 (m, 3H, CH_2, CH), 2.60 (t, *J* = 7.3 Hz, 2H, CH_2), 3.82–3.84 (m, 1H, H5′), 3.89–4.07 (m, 2H, H5″, H4′), 4.31 (dd, *J* = 12.1, 20.6 Hz, 1H, H3′), 6.24–6.26 (m, 1H, H1′), 7.49 (d, *J* = 7.6 Hz, 1H, H5), 8.34 (d, *J* = 7.6 Hz, 1H, H6); ^{13}C NMR δ 18.42, 24.96, 33.47, 60.50 (C5′), 68.14 (CH), 70.20 (C) 70.34 (t, *J* = 23.1 Hz, C3′), 82.35 (d, *J* = 8.6 Hz, C4′), 86.1 (dd, *J* = 26.6, 38.3 Hz, C1′), 96.30 (C5′), 123.91 (t, *J* = 259.3 Hz, C2′), 142.51 (C6), 157.78 (C2), 167.74 (C4), 175.97 (CO); ^{19}F NMR δ - 120.14 (d of m, *J* = 244.4 Hz, 1F), −119.23 (d of m, *J* = 243.6 Hz, 1F).

4-*N*-(7-Azidoheptanyl)-2′-deoxy-2′,2′-difluorocytidine (8)

Freshly prepared 7-Azido-1-aminoheptane (**S7**; 112.5 mg, 0.72 mmol) was added to a suspension of **7**[21] (100 mg, 0.24 mmol) in 1,4-dioxane (5 mL) and TEA (0.100 mL, 63 mg, 0.72 mmol) and the mixture was left stirring at 65°C. After 24 h, volatiles were evaporated and the resulting residue was column chromatographed (5% MeOH/$CHCl_3$) to give **8** (238 mg, 82%): UV (CH_3OH) λ max 267 nm (ε 8200), λ min 227 nm (ε 7400); ^{1}H NMR (CD_3OD) δ 1.31–1.41 (m, 6H, 3 × CH_2), 1.51–1.70 (m, 4H, 2 × CH_2), 3.25 (t, *J* = 6.9 Hz, 2H, CH_2), 3.45 (t, *J* = 7.0 Hz, 2H, CH_2) 3.77–3.83 (m, 1H, H5′), 3.91–3.99 (m, 2H, H5″, H4′), 4.25 (dt, *J* = 10.5, 20.8 Hz, 1H, H3′), 5.85 (d, *J* = 7.6 Hz, 1H, H5), 6.23–6.25 (m, 1H, H1′), 7.71 (d, *J* = 7.6 Hz, 1H, H6); ^{13}C NMR δ 27.75, 27.86, 29.84, 29.88, 29.92, 41.65, 52.45, 60.56 (C5′), 70.66 (t, *J* = 23.1 Hz, C3′), 82.22 (d, *J* = 8.6 Hz, C4′), 86.26 (dd, *J* = 26.6, 38.3 Hz, C1′), 97.32 (C5), 124.02 (t, *J* = 259.2 Hz, C2′), 140.80 (C6), 158.29 (C2), 165.38 (C4); ^{19}F NMR δ - 119.86 (d of m, *J* = 246.2 Hz, 1F), −119.89 (d of m, *J* = 240.2 Hz, 1F). HRMS (ESI+) m/z calcd for $C_{16}H_{25}F_2N_6O_4$ $[M+H]^+$ 403.1902; found 403.1913.

General procedure for click reactions

Sodium ascorbate (0.02 mmol), copper sulfate (0.02 mmol), nucleoside (0.1 mmol) and silicon-fluoride acceptor (0.1 mmol) were suspended in a mixture of *tert*-butanol/water (3:1 (v/v), 3 mL). The reaction mixture was left at room temperature for 1–6 hours. The reaction mixture was extracted with $CHCl_3$ (10 mL). The organic layer was washed with sat NH_4Cl (10 mL), brine (10 mL), dried over Na_2SO_4, filtered and evaporated under reduced pressure. The crude product was purified by chromatography ($CHCl_3$/MeOH 95:5) to afford the desired triazole adducts:

4-*N*-[4-(1-(4-(Diisopropylsilyl)benzyl)-1*H*-1,2,3-triazol-4-yl)butanoyl]-2′-deoxy-2′,2′difluorocytidine (4)—Treatment of **3** (35 mg, 0.1 mmol) with **S9** (24.7 mg, 0.1 mmol), as described in general procedure, gave **4** (52.6 mg, 87%). UV (CH_3OH) λ max

299 nm (ε 6700), 248 nm (ε 13000); ^{1}H NMR (CD_3CN) δ 0.96 (d, *J* = 7.3 Hz, 6H, *i*Pr), 1.03 (d, *J* = 7.3 Hz, 6H, *i*Pr), 1.18–1.20 (m, 4H, 2 × CH_2), 2.46 (t, *J* = 7.3 Hz, 2H, CH_2). 2.71 (t, *J* = 7.4 Hz, 2H, CH_2), 3.74–3.76 (m, 1H, H5′), 3.89–3.95 (m, 3H, H5″, H4′, Si-H), 4.24–4.26 (m, 1H, H3′), 5.50 (s, 2H, CH_2), 6.19 (t, *J* = 7.5 Hz, 1H, H1′), 7.28 (d, *J* = 8.0 Hz, 2H, Ar), 7.35 (d, *J* = 7.6 Hz, 1H, H5), 7.51 (d, *J* = 8.0 Hz, 2H, Ar), 7.56 (s, 1H), 8.10 (d, *J* = 7.6 Hz, 1H, H6); ^{13}C NMR δ 11.18, 18.65, 18.83, 24.96, 25.17, 37.04, 54.09, 59.93 (C5′), 69.68 (CH), 70.34 (t, *J* = 23.1 Hz, C3′), 81.82 (d, *J* = 8.6 Hz, C4′), 85.70 (dd, *J* = 26.6, 38.3 Hz, C1′), 97.03 (C5′), 122.39 (t, *J* = 259.3 Hz, C2′), 128.07, 134.96, 136.86, 138.11, 145.43 (C6), 148.04, 155.77 (C2), 163.85 (C4), 174.28 (CO); ^{19}F NMR δ - 120.10 (d of m, *J* = 233.4 Hz, 1F), −119.20 (d of m, *J* = 240.9 Hz, 1F). HRMS (ESI+) *m/z* calcd for $C_{28}H_{38}F_2N_6NaO_5Si$ $[M+Na]^+$ 627.2538; found 627.2522.

4-*N*-[11-(4-((4-(Diisopropylsilyl)benzyloxy)methyl)-1*H*-1,2,3-triazol-1-yl)undecanoyl]-2′-deoxy-2′,2′difluorocytidine (5)—Treatment of **2** (30 mg, 0.06 mmol) with **S10** (15.6 mg, 0.06 mmol), as described in general procedure, gave **5** (40.5 mg, 92%). UV (CH_3OH) λ max 299 nm (ε 6500), 250 nm (ε 12900), λ min 278 nm (ε 3800); ^{1}H NMR (CD_3CN) δ 0.96 (d, *J* = 7.3 Hz, 6H, *i*Pr), 1.05 (d, *J* = 7.3 Hz, 6H, *i*Pr), 1.24–1.47 (m, 14H, 7 × CH_2), 1.51–1.75 (m, 4H, 2 × CH_2), 2.38 (t, *J* = 7.3 Hz, 2H, CH_2), 3.81 (dd, *J* = 2.8, 12.4 Hz, 1H, H5′), 3.89–3.96 (m, 3H, H5″, H4′, Si-H), 4.30 (td, *J* = 8.5, 12.2 Hz, 1H, H3′), 4.33 (t, *J* = 7.1 Hz, 2H), 4.55 (s, 2H, CH_2), 4.61 (s, 2H, CH_2), 6.19 (t, *J* = 7.5 Hz, 1H, H1′), 7.33–7.35 (m, 3H, H5, Ar), 7.51 (d, *J* = 8.0 Hz, 2H, Ar), 7.74 (s, 1H), 8.10 (d, *J* = 7.6 Hz, 1H, H6); ^{13}C NMR δ 25.92, 27.80, 29.90, 30.11, 30.20, 30.33, 30.41, 30.50, 38.17, 52.47, 60.30 (C5′), 70.27 (dd, *J* = 22.2, 23.6 Hz, C3′), 82.92 (d, *J* = 8.6 Hz, C4′), 86.42 (dd, *J* = 26.6, 37.6 Hz, C1), 98.25 (C5), 120.87 (t, *J* = 259.9 Hz, C2′), 145.96 (C6), 157.68 (C2), 164.83 (C4), 176.00 (CO); ^{19}F NMR δ −120.09 (d of m, *J* = 239.2 Hz, 1F), −119.13 (d of m, *J* = 240.2 Hz, 1F). HRMS (ESI+) *m/z* calcd for $C_{36}H_{54}F_2N_6NaO$ Si $[M+Na]^+$ 6755.3738; found 755.3731.

4-*N*-[7-(4-((4-(Diisopropylsilyl)benzyloxy)methyl)-1*H*-1,2,3-triazol-1-yl)heptanyl]-2′-deoxy-2′,2′difluorocytidine (9)—Treatment of **8** (40 mg, 0.1 mmol) with **S10** (26.0 mg, 0.1mmol), as described in general procedure, gave **9** (59.6 mg, 90%). UV (CH_3OH) λ max 267 nm (ε 8200), λ min 228 nm (ε 7500); ^{1}H NMR (acetone-d_6) δ 0.99 (d, *J* = 7.3 Hz, 6H, *i*Pr), 1.05 (d, *J* = 7.3 Hz, 6H, *i*Pr), 1.31–1.41 (m, 10H, 5 × CH_2), 1.50–1.52 (m, 2H, CH_2), 1.90–1.93 (m, 2H, CH_2), 3.41–3.43 (m, 2H, CH_2), 3.80–3.82 (m, 1H, H5′), 3.91–4.02 (m, 3H, H5″, H4′, Si-H), 4.42–4.44 (m, 3H, H3′, CH_2), 4.60 (s, 2H, CH_2), 4.65 (s, 2H, CH_2), 5.82 (d, *J* = 7.6 Hz, 1H, H5), 6.23–6.25 (m, 1H, H1′), 7.38 (d, *J* = 8.0 Hz, 2H, Ar), 7.48 (d, *J* = 8.0 Hz, 2H, Ar), 7.71 (d, *J* = 7.6 Hz, 1H, H6), 7.99 (s, 1H, CH); ^{13}C NMR δ 11.26, 18.76, 18.96, 27.01, 27.34, 30.93, 40.97, 50.50, 60.31 (C5′), 64.42, 70.26 (t, *J* = 23.1 Hz, C3′), 72.37, 81.75 (d, *J* = 8.6 Hz, C4′), 84.92 (dd, *J* = 26.6, 38.3 Hz, C1′), 95.97 (C5′), 124.04 (t, *J* = 259.3 Hz, C2′), 127.88, 133.36, 140.78, 135.56, 136.34, 138.84, 140.78 (C6), 141.02, 155.92 (C2), 164.77 (C4); ^{19}F NMR δ −119.86 (d of m, *J* = 246.2 Hz, 1F), −119.89 (d of m, *J* = 240.2 Hz, 1F). HRMS (ESI+) *m/z* calcd for $C_{32}H_{48}F_2N_6NaO_5Si$ $[M+Na]^+$ 685.3322; found 685.3324.

General Procedure for Fluorination Reactions

Solid KF (4.7 mg, 0.08 mmol, 4 eq.) was added to a stirred solution of **5** (15 mg, 0.02 mmol,) and 18-Crown-6 ether (21 mg, 0.08 mmol, 4 eq.) in CH_3CN (3 mL) in a round bottom flask under N_2 atmosphere. To this mixture acetic acid (2 μL, 0.02 mmol. 1 eq.) was then added and the resulting reaction mixture was stirred at 80°C for 25 min. The reaction mixture was then left to cool (~5 min.) and filtered to remove the left over 18-crown ether and KF. The filtrate was washed with CH_3CN (2 mL) and the combined mother liquors were then concentrated under reduced pressure to give crude **6**. The resulting residue was chromatographed ($MeOH/CHCl_3$ 10:90) to give pure **9** (9.5 mg, 63%).

4-*N*-[11-(4-((4-(Fluorodiisopropylsilyl)benzyloxy)methyl)-1*H*-1,2,3-triazol-1-yl)undecanoyl]-2′-deoxy-2′,2′difluorocytidine (6)—Treatment of **5** (15 mg, 0.02 mmol) with KF (4.7 mg, 0.08 mmol), as described in general procedure, gave **6** (9.5 mg, 63%): UV (CH_3OH) λ max 299 nm (ε 6500), 250 nm (ε 12900), λ min 278 nm (ε 3800); ^{1}H NMR (CD_3OD) δ 0.99 (d, *J* = 7.3 Hz, 6H, *i*Pr), 1.07 (d, *J* = 7.3 Hz, 6H, *i*Pr), 1.24–1.47 (m, 14H, 7 × CH_2), 1.78–1.80 (m, 2H, CH_2), 1.90–1.92 (m, 2H, CH_2), 2.44 (t, *J* = 7.4 Hz, 2H, CH_2), 3.81 (dd, *J* = 2.8, 12.4 Hz, 1H, H5′), 3.89–3.99 (m, 2H, H5″, H4′), 4.29 (t, *J* = 10.4 Hz, 1H, H3′), 4.40 (t, *J* = 7.0 Hz, 2H), 4.60 (s, 2H, CH_2), 4.66 (s, 2H, CH_2), 6.26 (t, *J* = 7.5 Hz, 1H, H1′), 7.41 (d, *J* = 7.8 Hz, 2H, Ar), 7.49 (d, *J* = 7.6 Hz, H5), 7.54 (d, *J* = 8.1 Hz, 2H, Ar), 7.99 (s, 1H), 8.34 (d, *J* = 7.6 Hz, 1H, H6); ^{13}C NMR δ 13.22, 25.92, 27.80, 29.90, 30.11, 30.20, 30.33, 30.41, 30.50, 38.17, 52.47, 60.30 (C5′), 70.27 (dd, *J* = 22.2, 23.6 Hz, C3′), 82.92 (d, *J* = 8.6 Hz, C4′), 86.42 (dd, *J* = 26.6, 37.6 Hz, C1), 98.25 (C5), 120.87 (t, *J* = 259.9 Hz, C2′), 128.07, 135.53, 135.56, 136.34, 138.84, 145.93 (C6), 148.76, 145.93 (C6), 157.66 (C2), 164.78 (C4), 175.25 (CO); ^{19}F NMR δ - 188.86 (s, 1F), −120.09 (d of m, *J* = 239.2 Hz, 1F), −119.13 (d of m, *J* = 240.2 Hz, 1F). HRMS (ESI+) *m/z* calcd for $C_{36}H_{54}F_3N_6O_6Si$ $[M+H]^+$ 751.3821; found 751.3770.

4-*N*-[7-(4-((4-(Fluorodiisopropylsilyl)benzyloxy)methyl)-1*H*-1,2,3-triazol-1-yl)heptanyl]-2′-deoxy-2′,2′difluorocytidine (10)—Treatment of **9** (15 mg, 0.023 mmol) with KF (5.4 mg, 0.09 mmol), as described in general procedure, gave **10** (9 mg, 62 %): UV (CH_3OH) λ max 267 nm (ε 8200), λ min 228 nm (ε 7500); ^{1}H NMR (CD_3OD) δ 0.99 (d, *J* = 7.3 Hz, 6H, *i*Pr), 1.05 (d, *J* = 7.3 Hz, 6H, *i*Pr), 1.31–1.41 (m, 10H, 5 × CH_2), 1.50–1.52 (m, 2H, CH_2), 1.90–1.92 (m, 2H, CH_2), 3.38–3.40 (m, 2H, CH_2), 3.80–3.82 (m, 1H, H5′), 3.91–4.02 (m, 3H, H5″, H4′, Si-H), 4.24–4.26 (m, 1H, H3′), 4.41 (t, *J* = 6.9 Hz, 2H, CH_2), 4.60 (s, 2H, CH_2), 4.65 (s, 2H, CH_2), 5.82 (d, *J* = 7.6 Hz, 1H, H5), 6.21–6.23 (m, 1H, H1′), 7.41 (d, *J* = 8.0 Hz, 2H, Ar), 7.52 (d, *J* = 8.0 Hz, 2H, Ar), 7.71 (d, *J* = 7.6 Hz, 1H, H6), 8.01 (s, 1H, CH); ^{13}C NMR δ 11.26, 18.76, 18.96, 27.01, 27.34, 30.93, 40.97, 50.50, 60.31 (C5′), 64.42, 70.26 (t, *J* = 23.1 Hz, C3′), 72.37, 81.75 (d, *J* = 8.6 Hz, C4′), 84.92 (dd, *J* = 26.6, 38.3 Hz, C1′), 95.97 (C5′), 124.04 (t, *J* = 259.3 Hz, C2′), 127.88, 133.36, 140.78, 135.56, 136.34, 138.84, 140.78 (C6), 141.02, 155.92 (C2), 164.77 (C4). ^{19}F NMR δ - 188.82 (s, 1F), −119.75 (d of m, *J* = 244.1 Hz, 1F), −119.98 (d of m, *J* = 239.1 Hz, 1F). HRMS (ESI+) *m/z* calcd for $C_{32}H_{47}F_3N_6NaO_5Si$ $[M+Na]^+$ 703.3227; found 703.3234.

4-*N*-[4-(1-(4-(Fluorodiisopropylsilyl)benzyl)-1*H*-1,2,3-triazol-4-yl)butanoyl]-2′-deoxy-2′,2′difluorocytidine (11)—Treatment of **4** (15 mg, 0.025 mmol) with KF (5.9

mg, 0.1 mmol), as described in general procedure, gave **11** (10 mg, 65%): UV (CH_3OH) λ max 299 nm (ε 6700), 248 nm (ε 13000); ^{1}H NMR (CD_3OD) δ 0.99 (d, *J* = 7.3 Hz, 6H, *i*Pr), 1.06 (d, *J* = 7.3 Hz, 6H, *i*Pr), 1.18–1.20 (m, 2H, CH_2), 1.91–1.93 (m, 2H, CH_2), 2.50 (t, *J* = 7.3 Hz, 2H, CH_2). 2.78 (t, *J* = 7.4 Hz, 2H, CH_2), 3.82–3.84 (m, 1H, H5′), 3.93–4.05 (m, 2H, H5″, H4′), 4.29–4.31 (m, 1H, H3′), 5.59 (s, 2H, CH_2), 6.21 (t, *J* = 7.5 Hz, 1H, H1′), 7.35 (d, *J* = 7.9 Hz, 2H, Ar), 7.47 (d, *J* = 7.6 Hz, 1H, H5), 7.57 (d, *J* = 8.1 Hz, 2H, Ar), 7.81 (s, 1H), 8.33 (d, *J* = 7.6 Hz, 1H, H6); ^{13}C NMR δ 13.22, 13.35, 16.82, 17.01, 25.46, 25.53, 37.18, 54.70, 60.30 (C5′), 70.01 (CH), 70.34 (t, *J* = 23.1 Hz, C3′), 81.72 (d, *J* = 8.6 Hz, C4′), 82.92 (dd, *J* = 26.6, 38.3 Hz, C1′), 98.27 (C5′), 123.93 (t, *J* = 259.3 Hz, C2′), 128.39, 134.45, 135.53, 135.56, 136.34, 138.84, 145.93 (C6), 148.76, 157.66 (C2), 164.78 (C4), 175.25 (CO); ^{19}F NMR δ - 188.89 (s, 1F), −120.10 (d of m, *J* = 233.4 Hz, 1F), −119.20 (d of m, *J* = 240.9 Hz, 1F). HRMS (ESI+) *m/z* calcd for $C_{28}H_{37}F_3N_6NaO_5Si$ $[M+Na]^+$ 645.2445; found 645.2392.

Radiosynthesis of [^{18}F]Fluoro-silane probes

Unless otherwise stated, reagents and solvents were commercially available and used without further purification. Purification of [^{18}F]**10** was performed by semi-preparative HPLC using a WellChrom K-501 HPLC pump and reversed-phase Gemini-NX (5 μm, 10 × 250 nm, Phenomenex) column. Analytical HPLC was performed to confirm identity and radiochemical purity of the compound in a Knauer Smartline HPLC system with C18 reversed-phase Luna column (5 μm, 10 × 250 nm, Phenomenex). Radio-TLC was performed on precut silica plates (Baker-flex®, J.T.Baker). The radiochemical purity (RCP) was determined by using both radio-TLC and radio-HPLC radiation-detector chromatograms. For more detailed information, see supporting information.

[^{18}F]4-*N*-alkyl (10)

Microscale radiochemical synthesis: The microdroplet synthesis was performed using two Teflon-coated glass chips as shown in Figure S6 (see supporting information). The first was placed (Teflon-coated side up) on the heater. [^{18}F]fluoride in [^{18}O]H_2O (10μL; ~150 MBq [4 mCi]) was mixed with 12μL of a 70:30 v/v CH_3CN/H_2O solution containing K_{222} (0.23 μg) and K_2CO_3 (0.07 μg) and deposited in the center of the chip. Additional CH_3CN (10 μL) was added to aid in azeotropic drying, and the chip was heated at 105°C until the droplet on chip shrank to a small volume (~1μL). Next, 0.2 mg precursor **9** in 30 μL of DMSO with 1% v/v AcOH was added to the dried [^{18}F]KF/K_{222} residue, and the reaction droplet was covered with the second glass chip (Teflon-coated side down). Tape affixed to the edges of the top chip resulted in a gap of ~150 μm between the substrates. The chip was heated at 100°C for 20 min. Crude product was extracted from chip by adding 20 μL of 1:1 v/v MeOH:H_2O solution and then collecting the diluted mixture with a pipette. This process was repeated 2x for each substrate (~80 μL total volume). Without purification, the microscale synthesis took ~45 min. Decay-corrected crude radiochemical yield for 4-*N*-alkyl [^{18}F]**10** was 24.4 ± 4.1% (n=5).

Note: See supporting information for more detailed protocol and conventional synthesis.

Preclinical PET Imaging

Animal studies were approved by the UCLA Animal Research Committee and were carried out according to the guidelines of the Division of Laboratory Animal Medicine at UCLA.

PET/CT was performed on the Genisys 8 PET/CT (Sofie Biosciences, USA). The Genisys 8 PET/CT is an integrated scanner with a PET subsection that consists of 8 detectors with BGO scintillator array arranged in a box geometry and a back section consisting of a rotating CT gantry. For static PET scans, a WT C57BL/6 mouse was injected with approximately 75 μCi [^{18}F]**10** via tail vein. After 60 min of conscious uptake, mice were anesthetized with 1.5% isoflurane and placed in a dedicated imaging chamber. MicroPET images were acquired for 600 sec with an energy window of 150–650 keV, reconstructed using maximum-likelihood expectation maximization as recommended by the vendor. All images were corrected for CT-based photon attenuation, detector normalization and radioisotope decay (scatter correction was not applied) and converted to units of percent injected dose per gram (%ID/g). For dynamic PET scans, a WT C57BL/6 mouse was anesthetized with 2% isoflurane, placed in a dedicated imaging chamber with heating, and catheterized. Dynamic microPET imaging was started concurrently at the beginning of a 10 sec infusion via the catheter with approximately 75 μCi of [^{18}F]**10**. Data was acquired in listmode for 3600 sec with an energy window of 150–650 keV and histogrammed into a frame sequence of 4 × 15 sec, 8 × 30 sec, 5 × 60 sec, 4 × 300 sec, 3 × 600 sec. Images were reconstructed using maximum-likelihood expectation maximization as recommended by the vendor. All images were corrected for photon attenuation, detector normalization and radioisotope decay (scatter correction was not applied) and converted to units of percent injected dose per gram (%ID/g). All PET acquisitions were immediately followed by CT acquisition. The CT section consists of a gantry and flywheel that uses a 50 kVp, 200 uA x-ray source and flat-panel detector. The CT acquires images in a continuous-rotation mode and with standard CT acquisition time of 50 s. Standard scans are acquired with 720 projections at 55 ms per projection, and reconstructed using a Feldkamp algorithm.

Cytostatic activity assays

Murine leukemia L1210 cells were obtained from American Type Culture Collection (ATCC, Manassas, VA). The gemcitabine analogues tested (Table 2) were added to murine leukemia L1210 cell cultures in 96-well microtiter plates. After 72 h of incubation at 37 °C, the percentage surviving cells were assayed according to method described in the Cell Proliferaiton kit I (MTT) (Roche Biochemicals, Indianapolis, IN). The 50% and 75% inhibitory concentrations (IC_{50} and IC_{75}) were defined as the compound concentration required to inhibit cell proliferation by 50% and 75%, respectively.

Human HEK293 cells were obtained from ATCC (Manassas, VA). The gemcitabine analogues tested (**2**, **5**, **8** and **9**; Table 3) were added (50μM and 100 μM) to human HEK293 cell cultures in 12-well plates. After 48 h of incubation at 37 °C, the number of living cells was determined by MTT assays using Coulter counter.

Fluorescence studies with HEK293 cells

HEK293 cells were seeded in plates containing glass coverslips and incubated overnight. After incubation, fresh media solutions containing **8** (100 μM) was added and then incubated for various durations (6, 12 and 24 hr). Cells were fixed in paraformaldehyde (3.7%) for 15 min at room temperature, quenched, and washed with PBS as essentially described by Neef *et al.*[57]

Cells on coverslips were incubated upside-down with 50 μL of freshly prepared staining mix (10 μM Fluor alkyne, 1 mM CuSO4, and 10 mM sodium ascorbate in PBS) for 1 h at room temperature in the dark. Cells were then washed with 0.1% Triton X-100 and PBS, respectively. Cells were then stained with DAPI for 15 min at room temperature in the dark. After incubation, cells were washing with PBS and coverslips were mounted and viewed on an Olympus FV1200 Laser confocal microscope.

Supplementary Material

Refer to Web version on PubMed Central for supplementary material.

Acknowledgments

A.S. is supported by MBRS RISE program (NIGMS; R25 GM061347). This work was supported in part by the National Institutes of Health (R21 AG049918, P30 CA016042, T32 EB002101), and the UCLA Foundation from a donation made by Ralph and Marjorie Crump for the Crump Institute for Molecular imaging. The authors thank Dr. Roger Slavik and the staff of the UCLA Biomedical Cyclotron Facility for generously providing [^{18}F]fluoride for these studies, and Dr. Tove Olafsen and Charles Zamilpa of the Crump Institute's Preclinical Imaging Technology Center for assistance with PET/CT imaging.

Abbreviations

dFdC	2′,2′-difluoro-2′-deoxycytidine (Gemcitabine)
hENT1	human equilibrative nucleoside transport protein 1
dCK	deoxycytidine kinase
dFdU	2′,2′-difluorouridine
CDA	cytidine deaminase
[^{18}F]FAC	1-(2-deoxy-2-[^{18}F]fluoro-β-D-arabinofuranosyl)cytosine
EDC	*N*-dimethylaminopropyl)-*N*′-ethyl-carbodiimide
HOBt	1-hydroxybenzotriazole
DIPEA	*N, N*-Diisopropylethylamine
TEA	triethylamine

References

1. Toschi L, Finocchiaro G, Bartolini S, Gioia V, Cappuzzo F. Role of gemcitabine in cancer therapy. Future Oncol. 2005; 1:7–17. [PubMed: 16555971]

2. Mackey JR, Mani RS, Selner M, Mowles D, Young JD, Belt JA, Crawford CR, Cass CE. Functional Nucleoside Transporters Are Required for Gemcitabine Influx and Manifestation of Toxicity in Cancer Cell Lines. Cancer Res. 1998; 58:4349–4357. [PubMed: 9766663]

3. Heinemann V, Hertel LW, Grindey GB, Plunkett W. Comparison of the Cellular Pharmacokinetics and Toxicity of 2′,2′-Difluorodeoxycytidine and 1-β-Arabinofuranosylcytosine. Cancer Res. 1988; 48:4024–4031. [PubMed: 3383195]

4. Huang P, Chubb S, Hertel LW, Grindey GB, Plunkett W. Action of 2′,2′-Difluorodeoxycytidine on DNA Synthesis. Cancer Res. 1991; 51:6110–6117. [PubMed: 1718594]

5. Shipley LA, Brown TJ, Cornpropst JD, Hamilton M, Daniels WD, Culp HW. Metabolism and disposition of gemcitabine, and oncolytic deoxycytidine analog, in mice, rats, and dogs. Drug Metab Dispos. 1992; 20:849–855. [PubMed: 1362937]

6. Hodge LS, Taub ME, Tracy TS. The Deaminated Metabolite of Gemcitabine, 2′,2′-Difluorodeoxyuridine, Modulates the Rate of Gemcitabine Transport and Intracellular Phosphorylation via Deoxycytidine Kinase. Drug Metab Dispos. 2011; 39:2013–2016. [PubMed: 21832002]

7. Veltkamp SA, Pluim D, van Eijndhoven MAJ, Bolijn MJ, Ong FHG, Govindarajan R, Unadkat JD, Beijnen JH, Schellens JHM. New insights into the pharmacology and cytotoxicity of gemcitabine and 2′,2′-difluorodeoxyuridine. Mol Cancer Ther. 2008; 7:2415–2425. [PubMed: 18723487]

8. Couvreur P, Stella B, Reddy LH, Hillaireau H, Dubernet C, Desmaële D, Lepêtre-Mouelhi S, Rocco F, Dereuddre-Bosquet N, Clayette P, Rosilio V, Marsaud V, Renoir JM, Cattel L. Squalenoyl Nanomedicines as Potential Therapeutics. Nano Lett. 2006; 6:2544–2548. [PubMed: 17090088]

9. Bender DM, Bao J, Dantzig AH, Diseroad WD, Law KL, Magnus NA, Peterson JA, Perkins EJ, Pu YJ, Reutzel-Edens SM, Remick DM, Starling JJ, Stephenson GA, Vaid RK, Zhang D, McCarthy JR. Synthesis, Crystallization, and Biological Evaluation of an Orally Active Prodrug of Gemcitabine. J Med Chem. 2009; 52:6958–6961. [PubMed: 19860433]

10. Vandana M, Sahoo SK. Long circulation and cytotoxicity of PEGylated gemcitabine and its potential for the treatment of pancreatic cancer. Biomaterials. 2010; 31:9340–9356. [PubMed: 20851464]

11. Bergman AM, Adema AD, Balzarini J, Bruheim S, Fichtner I, Noordhuis P, Fodstad Ø, Myhren F, Sandvold ML, Hendriks HR, Peters GJ. Antiproliferative activity, mechanism of action and oral antitumor activity of CP-4126, a fatty acid derivative of gemcitabine, in in vitro and in vivo tumor models. Invest New Drug. 2011; 29:456–466.

12. Moysan E, Bastiat G, Benoit JP. Gemcitabine versus Modified Gemcitabine: A Review of Several Promising Chemical Modifications. Mol Pharm. 2013; 10:430–444. [PubMed: 22978251]

13. Tsume Y, Drelich AJ, Smith DE, Amidon GL. Potential Development of Tumor-Targeted Oral Anti-Cancer Prodrugs: Amino Acid and Dipeptide Monoester Prodrugs of Gemcitabine. Molecules. 2017; 22doi: 10.3390/molecules22081322

14. Vale N, Ferreira A, Fernandes I, Alves C, Araujo MJ, Mateus N, Gomes P. Gemcitabine anti-proliferative activity significantly enhanced upon conjugation with cell-penetrating peptides. Bioorg Med Chem Lett. 2017; 27:2898–2901. [PubMed: 28495087]

15. Ferraboschi P, Ciceri S, Grisenti P. Synthesis of Antitumor Fluorinated Pyrimidine Nucleosides. Org Prep Proced Int. 2017; 49:69–154.

16. Dasari M, Acharya AP, Kim D, Lee S, Lee S, Rhea J, Molinaro R, Murthy N. H-Gemcitabine: A New Gemcitabine Prodrug for Treating Cancer. Bioconjugate Chem. 2013; 24:4–8.

17. Maiti S, Park N, Han JH, Jeon HM, Lee JH, Bhuniya S, Kang C, Kim JS. Gemcitabine–Coumarin–Biotin Conjugates: A Target Specific Theranostic Anticancer Prodrug. J Am Chem Soc. 2013; 135:4567–4572. [PubMed: 23461361]

18. Yang Z, Lee JH, Jeon HM, Han JH, Park N, He Y, Lee H, Hong KS, Kang C, Kim JS. Folate-Based Near-Infrared Fluorescent Theranostic Gemcitabine Delivery. J Am Chem Soc. 2013; 135:11657–11662. [PubMed: 23865715]

19. Liu LH, Qiu WX, Li B, Zhang C, Sun LF, Wan SS, Rong L, Zhang XZ. A Red Light Activatable Multifunctional Prodrug for Image-Guided Photodynamic Therapy and Cascaded Chemotherapy. Adv Funct Mater. 2016; 26:6257–6269.

20. Maiti S, Paira P. Biotin conjugated organic molecules and proteins for cancer therapy: A review. Eur J Med Chem. 2018; 145:206–223. [PubMed: 29324341]
21. Pulido J, Sobczak AJ, Balzarini J, Wnuk SF. Synthesis and Cytostatic Evaluation of 4-N-Alkanoyl and 4-N-Alkyl Gemcitabine Analogues. J Med Chem. 2014; 57:191–203. [PubMed: 24341356]
22. Pulido, J. Ph D. Florida International University; 2014. Design and Synthesis of 4-N-Alkanoyl and 4-N-Alkyl Gemcitabine Analogues Suitable for Positron Emission Tomography.
23. Alauddin MM. Positron emission tomography (PET) imaging with (18)F-based radiotracers. Am J Nucl Med Mol Img. 2012; 2:55–76.
24. Jacobson O, Kiesewetter DO, Chen X. Fluorine-18 Radiochemistry, Labeling Strategies and Synthetic Routes. Bioconjugate Chem. 2015; 26:1–18.
25. Taylor NJ, Emer E, Preshlock S, Schedler M, Tredwell M, Verhoog S, Mercier J, Genicot C, Gouverneur V. Derisking the Cu-Mediated 18F-Fluorination of Heterocyclic Positron Emission Tomography Radioligands. J Am Chem Soc. 2017; 139:8267–8276. [PubMed: 28548849]
26. Campbell MG, Mercier J, Genicot C, Gouverneur V, Hooker JM, Ritter T. Bridging the gaps in 18F PET tracer development. Nat Chem. 2017; 9:1–3.
27. Neumann CN, Hooker JM, Ritter T. Concerted nucleophilic aromatic substitution with 19F− and 18F−. Nature. 2016; 534:369–373. [PubMed: 27281221]
28. Hoover AJ, Lazari M, Ren H, Narayanam MK, Murphy JM, van Dam RM, Hooker JM, Ritter T. A Transmetalation Reaction Enables the Synthesis of [18F]5-Fluorouracil from [18F]Fluoride for Human PET Imaging. Organometallics. 2016; 35:1008–1014. [PubMed: 27087736]
29. Hertel LW, Kroin JS, Misner JW, Tustin JM. Synthesis of 2-deoxy-2,2-difluoro-D-ribose and 2-deoxy-2,2′-difluoro-D-ribofuranosyl nucleosides. J Org Chem. 1988; 53:2406–2409.
30. Brown K, Dixey M, Weymouth-Wilson A, Linclau B. The synthesis of gemcitabine. Carbohydr Res. 2014; 387:59–73. [PubMed: 24636495]
31. Synthesis of 2′-[18F]-labelled gemcitabine from the protected 2′-ketouridine or 2′-ketocytidine employing deoxodifluorination method with DAST/[18F]fluoride/K222 were attempted but gave mono 18F-labeled gemcitabine in very low radiochemical yield (0.2–0.3%) and reproducibility: Meyer, J.-P. Synthetic Routes to 18F-labelled gemcitabine and related 2′-fluoronucleosides. Ph.D., Cardiff University, 2014
32. Radu CG, Shu CJ, Nair-Gill E, Shelly SM, Barrio JR, Satyamurthy N, Phelps ME, Witte ON. Molecular imaging of lymphoid organs and immune activation by positron emission tomography with a new [18F]-labeled 2′-deoxycytidine analog. Nat Med. 2008; 14:783–788. [PubMed: 18542051]
33. Laing RE, Walter MA, Campbell DO, Herschman HR, Satyamurthy N, Phelps ME, Czernin J, Witte ON, Radu CG. Noninvasive prediction of tumor responses to gemcitabine using positron emission tomography. Proc Natl Acad Sci USA. 2009; 106:2847–2852. [PubMed: 19196993]
34. Lee JT, Campbell DO, Satyamurthy N, Czernin J, Radu CG. Stratification of Nucleoside Analog Chemotherapy Using 1-(2′-Deoxy-2′-18F-Fluoro-β-d-Arabinofuranosyl)Cytosine and 1-(2′-Deoxy-2′-18F-Fluoro-β-l-Arabinofuranosyl)-5-Methylcytosine PET. J Nucl Med. 2012; 53:275–280. [PubMed: 22302964]
35. Artin E, Wang J, Lohman GJS, Yokoyama K, Yu G, Griffin RG, Bar G, Stubbe J. Insight into the Mechanism of Inactivation of Ribonucleotide Reductase by Gemcitabine 5′-Diphosphate in the Presence or Absence of Reductant. Biochemistry. 2009; 48:11622–11629. [PubMed: 19899770]
36. Gens TA, Wethongton JA, Brosi AR. The Exchange of F18between Metallic Fluorides and Silicon Tetrafluoride. J Phys Chem. 1958; 62:1593–1593.
37. Winfield JM. Preparation and use of 18-fluorine labelled inorganic compounds. J Fluorine Chem. 1980; 16:1–17.
38. Rosenthal MS, Bosch AL, Nickles RJ, Gatley SJ. Synthesis and some characteristics of no-carrier added [18F]fluorotrimethylsilane. Int J Appl Radiat Is. 1985; 36:318–319.
39. Mu L, Hohne A, Schubiger PA, Ametamey SM, Graham K, Cyr JE, Dinkelborg L, Stellfeld T, Srinivasan A, Voigtmann U, Klar U. Silicon-based building blocks for one-step 18F-radiolabeling of peptides for PET imaging. Angew Chem Int Ed Engl. 2008; 47:4922–4925. [PubMed: 18496798]

40. Schirrmacher R, Bradtmöller G, Schirrmacher E, Thews O, Tillmanns J, Siessmeier T, Buchholz HG, Bartenstein P, Wängler B, Niemeyer CM, Jurkschat K. 18F-Labeling of Peptides by means of an Organosilicon-Based Fluoride Acceptor. Angew Chem, Int Ed. 2006; 45:6047–6050.
41. Choudhry U, Martin KE, Biagini S, Blower PJ. A49 Alkoxysilane groups for instant labelling of biomolecules with 18F. Nucl Med Commun. 2006; 27:293.
42. Schulz J, Vimont D, Bordenave T, James D, Escudier JM, Allard M, Szlosek-Pinaud M, Fouquet E. Silicon-Based Chemistry: An Original and Efficient One-Step Approach to [18F]-Nucleosides and [18F]-Oligonucleotides for PET Imaging. Chem Eur J. 2011; 17:3096–3100. [PubMed: 21312302]
43. Dialer LO, Selivanova SV, Muller CJ, Muller A, Stellfeld T, Graham K, Dinkelborg LM, Kramer SD, Schibli R, Reiher M, Ametamey SM. Studies toward the development of new silicon-containing building blocks for the direct (18)F-labeling of peptides. J Med Chem. 2013; 56:7552–7563. [PubMed: 23992105]
44. Menard-Moyon C, Ali-Boucetta H, Fabbro C, Chaloin O, Kostarelos K, Bianco A. Controlled Chemical Derivatisation of Carbon Nanotubes with Imaging, Targeting, and Therapeutic Capabilities. Chem Eur J. 2015; 21:14886–14892. [PubMed: 26331300]
45. Keng PY, Chen S, Ding H, Sadeghi S, Shah GJ, Dooraghi A, Phelps ME, Satyamurthy N, Chatziioannou AF, Kim CJC, van Dam RM. Micro-chemical synthesis of molecular probes on an electronic microfluidic device. Proc Natl Acad Sci USA. 2012; 109:690–695. [PubMed: 22210110]
46. Keng PY, Dam RMv. Digital Microfluidics: A New Paradigm for Radiochemistry. Mol Imaging. 2015; 14:579–594.
47. Jordheim LP, Cros E, Gouy MH, Galmarini CM, Peyrottes S, Mackey J, Perigaud C, Dumontet C. Characterization of a Gemcitabine-Resistant Murine Leukemic Cell Line. Clin Cancer Res. 2004; 10:5614–5621. [PubMed: 15328204]
48. Sigmond J, Honeywell RJ, Postma TJ, Dirven CMF, de Lange SM, van der Born K, Laan AC, Baayen JCA, Van Groeningen CJ, Bergman AM, Giaccone G, Peters GJ. Gemcitabine uptake in glioblastoma multiforme: potential as a radiosensitizer. Ann Oncol. 2009; 20:182–187.
49. Cividini F, Filoni DN, Pesi R, Allegrini S, Camici M, Tozzi MG. IMP–GMP specific cytosolic 5′-nucleotidase regulates nucleotide pool and prodrug metabolism. Biochim Biophys Acta. 2015; 1850:1354–1361. [PubMed: 25857773]
50. Zauri M, Berridge G, Thezenas ML, Pugh KM, Goldin R, Kessler BM, Kriaucionis S. CDA directs metabolism of epigenetic nucleosides revealing a therapeutic window in cancer. Nature. 2015; 524:114–118. [PubMed: 26200337]
51. Mahfouz RZ, Jankowska A, Ebrahem Q, Gu X, Visconte V, Tabarroki A, Terse P, Covey J, Chan K, Ling Y, Engelke KJ, Sekeres MA, Tiu R, Maciejewski J, Radivoyevitch T, Saunthararajah Y. Increased CDA Expression/Activity in Males Contributes to Decreased Cytidine Analog Half-Life and Likely Contributes to Worse Outcomes with 5-Azacytidine or Decitabine Therapy. Clin Cancer Res. 2013; 19:938–948. [PubMed: 23287564]
52. Weizman N, Krelin Y, Shabtay-Orbach A, Amit M, Binenbaum Y, Wong RJ, Gil Z. Macrophages mediate gemcitabine resistance of pancreatic adenocarcinoma by upregulating cytidine deaminase. Oncogene. 2014; 33:3812–3819. [PubMed: 23995783]
53. Ebrahem Q, Mahfouz R, Ng KP, Saunthararajah Y. High cytidine deaminase expression in the liver provides sanctuary for cancer cells from decitabine treatment effects. Oncotarget. 2012; 3:1137–1145. [PubMed: 23087155]
54. Krajewska E, Shugar D. Alkylated cytosine nucleosides: substrate and inhibitor properties in enzymatic deamination. Acta Biochim Pol. 1975; 22:185–194. [PubMed: 1098340]
55. The logP of the 4-*N*-alkyl analogues calculated using ChemBioDraw showed high lipophilicity (e.g. **8**, 3.55; **9** 4.72; **10**, 4.72).
56. Also HPLC analysis of cell lysates after incubation of HEK293 cells with 8 for 24 h, showed that 4-N-alkyl analogue 8 is incorporated into the cell, and stays intact: Gonzalez, C. Synthesis of Gemcitabine Analogues with Silicon-Fluoride Acceptors for 18F Labeling. Ph.D., Florida International University
57. Neef AB, Luedtke NW. An Azide-Modified Nucleoside for Metabolic Labeling of DNA. ChemBioChem. 2014; 15:789–793. [PubMed: 24644275]

HIGHLIGHTS

- Gemcitabine analogs with silicon-based building blocks are efficiently ^{18}F-labeled
- 4-*N*-acyl analogs had stronger antiproliferative activity than 4-*N*-alkyl analogs
- 4-*N*-alkyl analogs have better chemical stability than 4-*N*-acyl counterparts
- PET imaging in mice showed initial concentration of ^{18}F in liver and kidneys

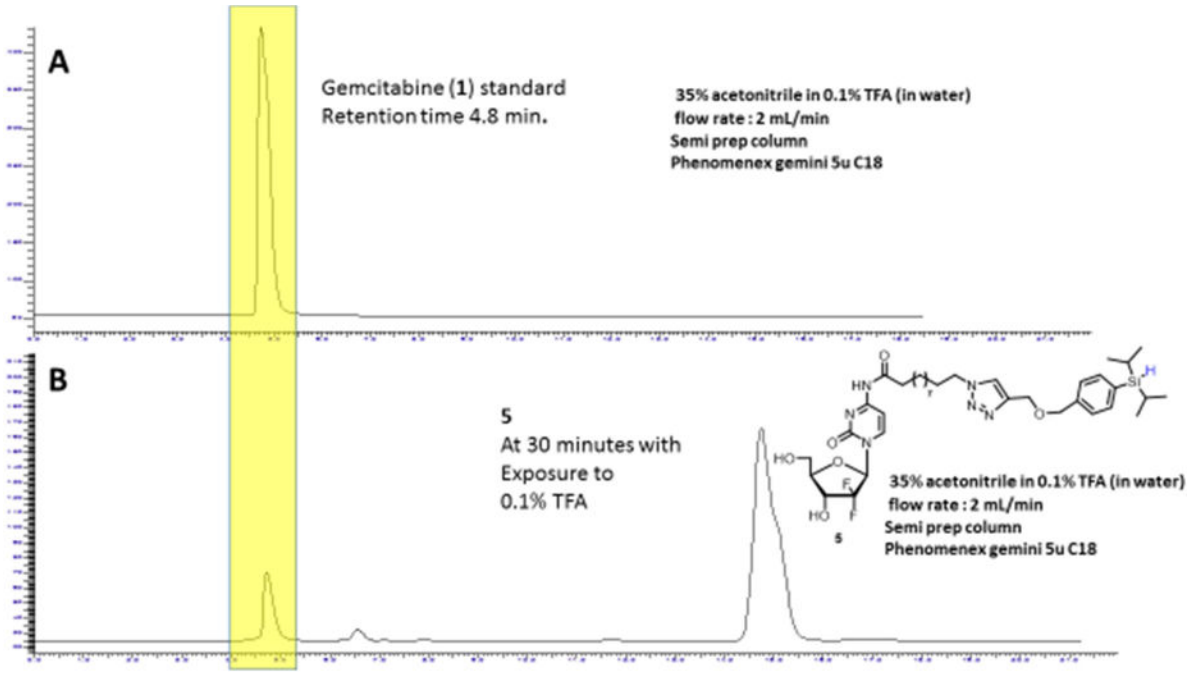

Figure 1.

Stability of 4-*N*-alkanoyl **5** (*chromatogram A:* ***1****, chromatogram B:* ***5*** *after 30 min*) in 35 %CH_3CN/0.1% TFA

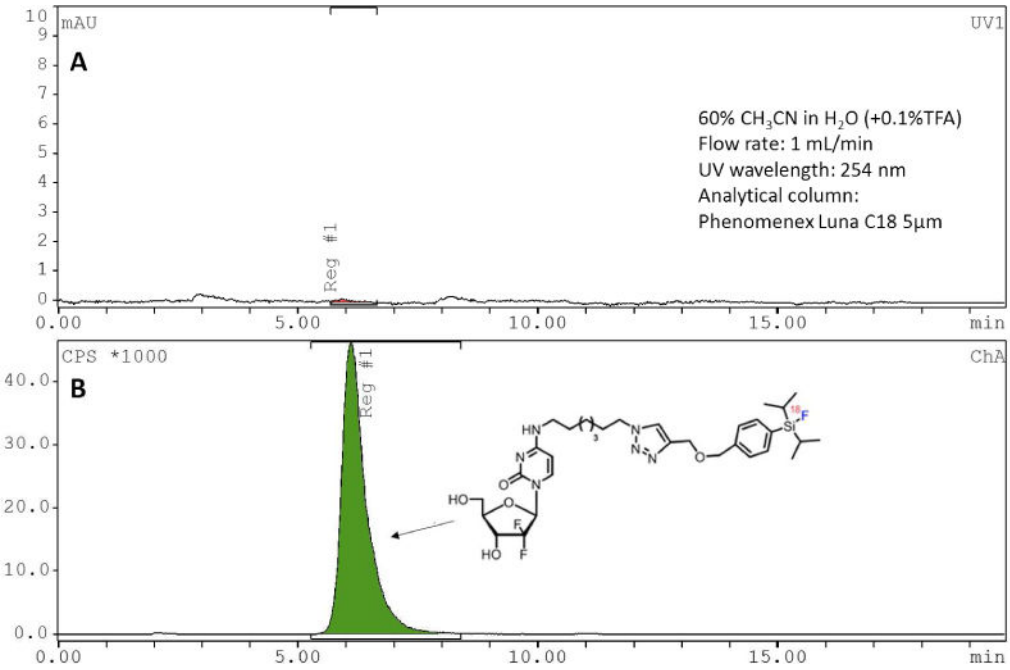

Figure 2.

Analytical HPLC chromatogram of purified 4-*N*-alkyl [^{18}F]**10** (produced at conventional scale) (chromatogram **A**: UV detector, chromatogram **B**: gamma detector).

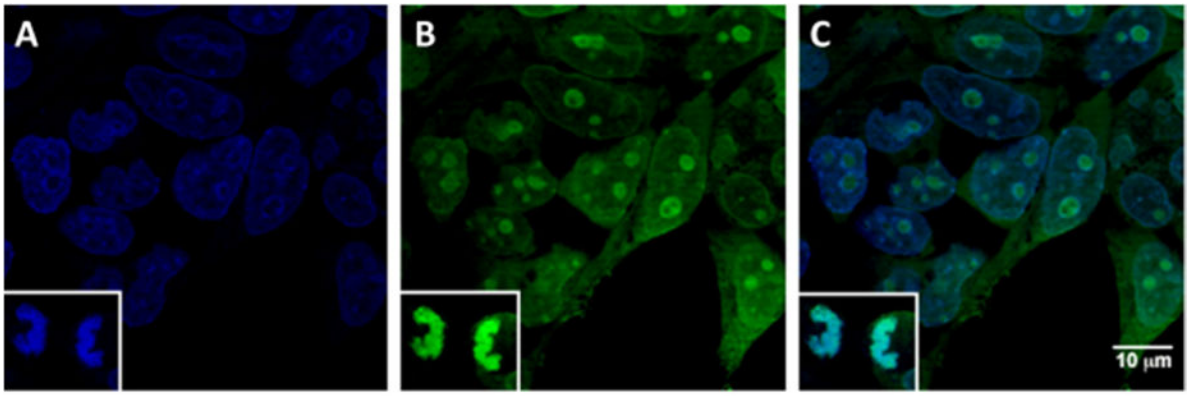

Figure 3.

Incorporation of **8** in HEK293 cells after 24 h, followed by fixation and addition of Fluor 488-Alkyne and copper (I): A) Nuclear staining with DAPI, B) Cell staining with Fluor 488-Alkyne. C) Merged A & B microscopy images. Inset: Staining of DNA during cell division. Scale bars: 10 μm.

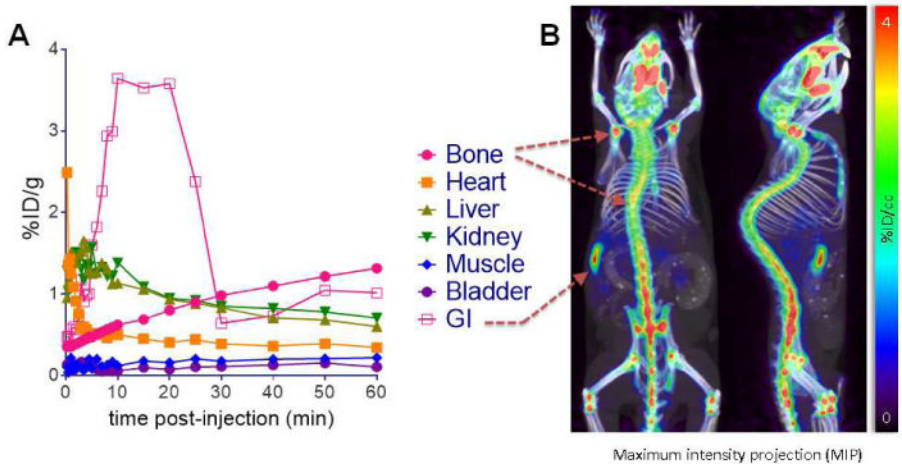

Figure 4.

(Left) Dynamic biodistribution of [^{18}F]**10** in WT C57BL/6 mouse. (Right) Maximum intensity projection at 1 h post-injection (left: coronal; right: sagittal).

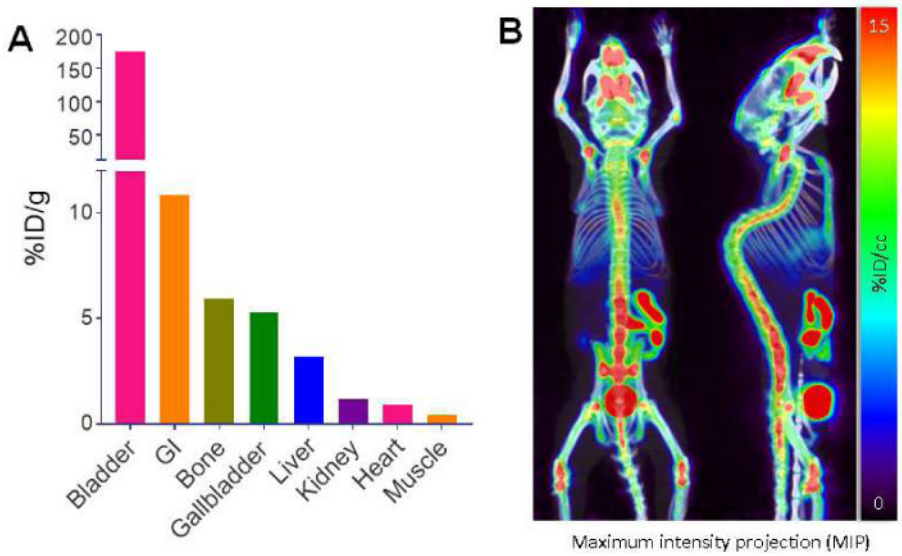

Figure 5.

(Left) Biodistribution of [^{18}F]**10** from 10 min static scan in WT C57BL/6 mouse at 1 h post-injection. (Right) Maximum intensity projection of 10 min static scan at 1 h post-injection (left: coronal; right: sagittal).

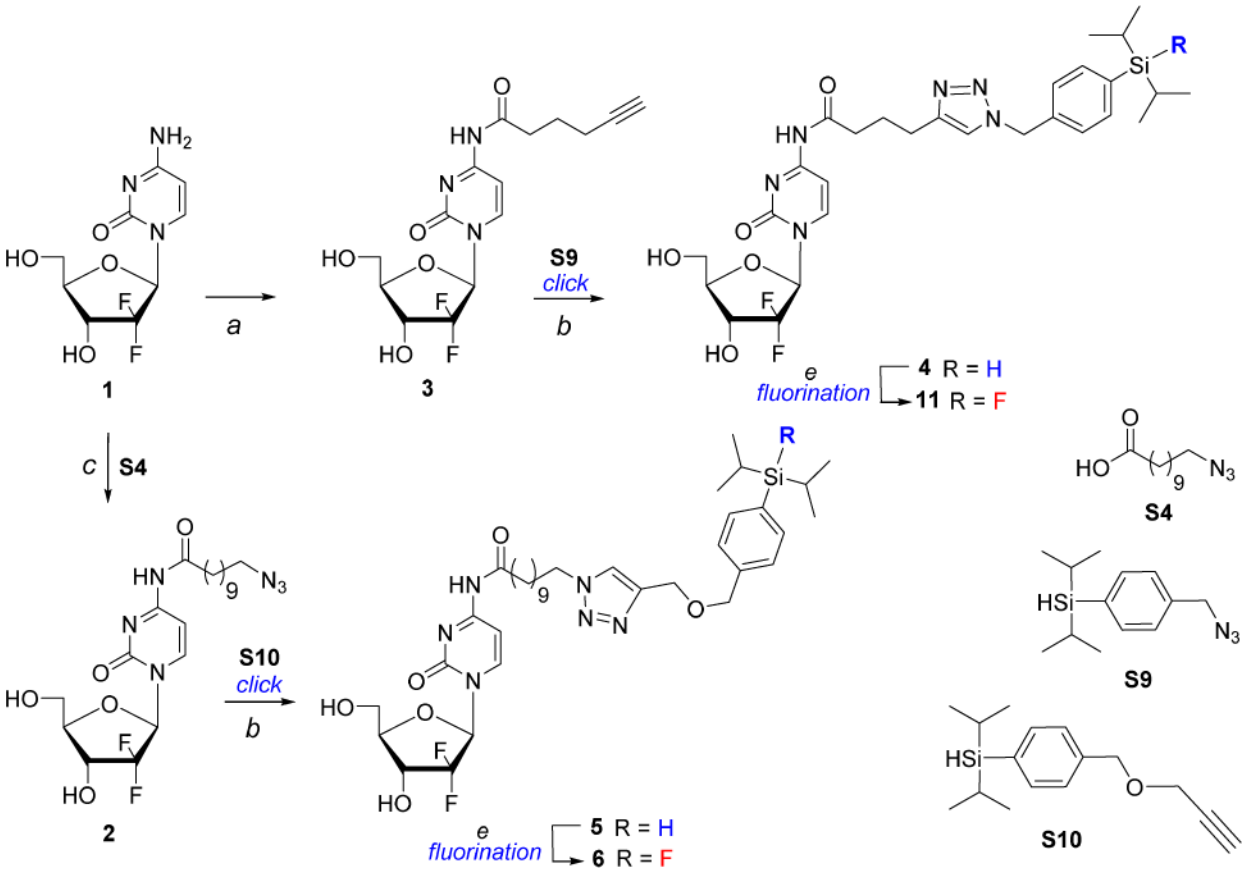

Scheme 1.

Synthesis of 4-*N*-alkanoyl gemcitabine analogues with silicon-fluoride acceptors.[a]

[a]Reagents and conditions: (a) (i) TMSCl/Pyr/MeCN, 3 h, (ii) $CH{\equiv}C(CH_2)_3COOH$/EDC/MeCN/60°C; (iii) EtOH, 45°C, 4 h; (b) Sodium ascorbate/Cu_2SO_4/*t*-BuOH/water (3:1), 6 h; (c) HOBt/DIPEA/EDC/DMF/65 °C/overnight; (d) KF/18-crown-6/AcOH/MeCN/80 °C/25 min. Synthesis and chemical characterization of substrates **S4**, **S9** and **S10** are described in SI Section.

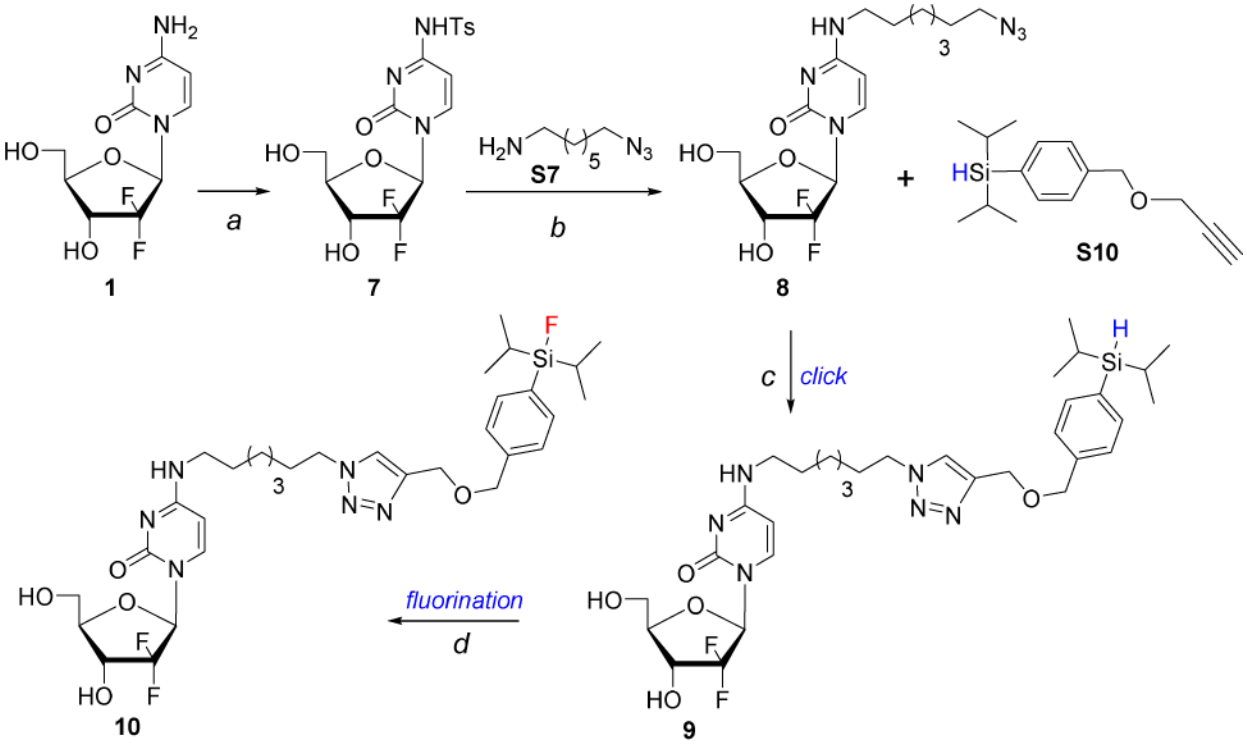

Scheme 2.

Synthesis of 4-*N*-alkyl gemcitabine analogues with silicon-fluoride acceptors.[a]

[a]Reagents and conditions: (a) (i) TMSCl/Pyr, (ii) TsCl, (iii) MeOH/NH_3; (b) TEA/1,4-dioxane/65 °C; (c) Sodium ascorbate/Cu_2SO_4/*t*-BuOH/H_2O (3:1)/6 h; (d) KF/18-crown-6/AcOH/MeCN/80°C/25 min.

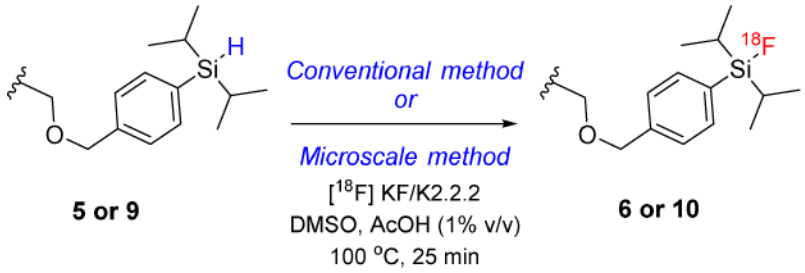

Scheme 3.

Radiosynthesis of [^{18}F] 4-*N*-alkanoyl and alkyl gemcitabine analogues with silicon-fluoride acceptors.

Table 1

^{18}F radiosynthetic yields of 4-*N*-modified gemcitabine analogues **6** and **10**.

Entry	Analogue	Conventional radiosynthesis[a]	Microscale radiosynthesis[b]
		Average decay-corrected isolated RCY (%)	Decay-corrected crude RCY (%)
1	**6**	0.5	10
2	**10**	6.6 ± 3.2 (n=5)	24.4 ± 4.1 (n=5)

[a] 2–3 mg scale reactions

[b] 0.2 mg scale reactions

Table 2

In vitro cytostatic activity of 4-*N*-modified gemcitabine analogues in L1210 lymphocytic leukemia cell line.

Compounds	IC_{50} (μM)[a]	IC_{75} (μM)[a]
2	8.0 ±0.4	14.9± 2.4
3	65.3±0.6	88.3±1.1
5	7.5±0.4	13.3±1.1
6	40.0±1.9	78.3±5.6
8	>200	>200
9	>200	>200

[a]Values are the mean of three independent experiments and reported as mean ± SD.

Table 3

In vitro inhibitory activity of gemcitabine and 4-N-modified gemcitabine analogues (at 50 and 100 μM concentrations) in human embryonic kidney HEK293 cell line.

Compounds	% inhibition (50 μM)[a]	% inhibition (100 μM)[a]
1	38±4%	45±6%
2	79±10%	89±15%
5	42±5%	63±6%
8	45±9%	61±11%
9	50±9%	78±15%

[a]Values are the mean of three independent experiments and reported as mean ± SD.